Fast and efficient direct formation of size-controlled nanostructures of coordination polymers based on copper(I)-iodine bearing functional pyridine terminal ligands

Javier Conesa-Egea,[a] Khaled Hassanein,[a] Marta Muñoz,[b] Félix Zamora,[a,c,d*] Pilar Amo-Ochoa[a,d*]

We report on the direct formation of 1D nanostructures of two coordination polymers based on copper(I)-iodine double chains decorated with ethyl isonicotinate or 2-amino-5-nitropyridine as terminal ligands. The use of different reaction conditions, e.g. energy of the formation process, solvents, and/or concentration of reactants, have allowed to control the size of the fibres and ribbons directly formed in this process going from micron- to submicron- up to nano-size. We show experiments that direct the formation of materials kinetically *versus* thermodinamically controlled, adjusting simple experimental parameters. Finally, a morphological study on the Cu(I)-iodine bearing 2-amino-5-nitropyridine nanofibres has confirmed their reversible molecular recognition ability towards acetic acid vapours.

Introduction

Coordination polymers (CPs) encompass a large family of compounds, formed by central metal ions and ligands linked by coordination bonds. Depending on the selected building blocks, CPs give rise to mono, bi or three-dimensional structures. Additionally, the mono- and bi-dimensional structures can extend their networks using supramolecular interactions such as hydrogen bonds or weak interactions such as Van der Waals forces. The building blocks are also determining for the physical and chemical properties of the CPs, suitable combinations give rise to multifunctional or even stimuli response materials.[1-3] Thus, CPs decorated with specific organic ligands functionalized with donor-acceptor H-bond groups can incorporate molecular recognition capabilities, hence their potential sensing applications.[4-6] Additionally, these functional organic ligands with intrinsic self-assembly capabilities will direct the three-dimensional network and function of CPs, since new intermolecular hydrogen bonds involving the CPs and/or with other molecules will be stablished. This new scenery is also promising to define novel sensors based on CPs.[7] However, the number of CPs decorated with donor-acceptor groups is still scarce.[8-11,12-15]

Additionally, in this context the study of the materials at the nanoscale increases their potential applications, for instance, giving the possibility to fabricate ultrasensitive sensors based on CP nanostructures. Indeed, this is an interesting aspect towards the use of materials as biological sensors. Therefore, the development of methods for controlling the CP size is a key prerequisite to gain access to a plethora of interesting properties and size-dependent phenomena inherent to CP nanomaterials. In this regard, CPs seem to have, among other interesting advantages, an intrinsic facility to be nanoprocessed, based on the reversible nature of the constituent bonds, coordination bonds.[16-20] Thus, in the last years, several CP nanostructures have been obtained using different strategies such as fast-precipitation, interfacial synthesis, hydro-solvothermal, microemulsions or liquid phase exfoliation.[21] It is worth mentioning that a small change in the concentration of the reactants, or the addition of a poor solvent to the reaction medium, is sometimes enough to produce a significant change in the size of the final material going from the micron- to the nano-scale. Thus, for instance, in some cases the high insolubility in the reaction medium of the CPs gives rise to their fast precipitation as nanocrystals. However, there are not many studies taking advantage of the facility to create CP nanostructures using these bottom-up

a. Departamento de Química Inorgánica, Universidad Autónoma de Madrid, 28049 Madrid, Spain. E-mail: pilar.amo@uam.es.

b. Departamento de Ciencia e Ingeniería de Materiales, Universidad Rey Juan Carlos, Madrid, Spain.

c. Matter Physics Center (IFIMAC), Universidad Autónoma de Madrid, 28049 Madrid, Spain.

d. Institute for Advanced Research in Chemical Sciences (IAdChem), Universidad Autónoma de Madrid, 28049 Madrid, Spain.

approaches and/or analysing their properties at the nanoscale.[22]

Here we report on an easy, low cost and fast procedure to reduce the size from micron- to sub-micron and to the nano-scale of two different CPs based on copper(I)-iodine double chains bearing either ethyl isonicotinate (EtIN), which presents optical properties,[23] or 2-amino-5-nitropyridine (ANP), a terminal ligand with molecular recognition capabilities.[6, 24] The syntheses of these two CPs have been optimized varying different experimental parameters (reaction time, solvents, reactant concentration…) to produce nanostructures with control in the size and shape, so as to find the optimal conditions at which de size reduction is greatest. Finally, a study of the morphological changes induced by the presence of acetic acid vapours in the copper(I)-iodine double chains bearing 2-amino-5-nitropyridine (ANP) CP has been carried out.

Figure 1. (a) Structure of $[Cu(\mu_3\text{-}I)(ANP)]_n$ (**1m**) chain. Grey: C; white: H; blue: N; red: O; orange: Cu; purple: I. SEM images of microcrystals of $[Cu(\mu_3\text{-}I)(ANP)]_n$ (**1m**) (b) and nanofibres prepared by magnetic stirring at 500 rpm (**1n**) (c). AFM image of **1n** fibres (d) and their height profiles (insets).

Results and discussion

Slow evaporation, between three days and a week, at room temperature of the mother liquor obtained from the direct reaction between CuI and EtIN or ANP in acetonitrile, gives rise to the formation of microcrystals of both $[Cu(\mu_3\text{-}I)(ANP)]_n$ (**1m**) (ANP= 2-amino-5-nitropyridine) with dimensions of 22 ± 12 μm width and 1.0 ± 0.5 mm length, and of $[Cu(\mu_3\text{-}I)(EtIN)]_n$ (**2m**) (EtIN= ethyl isonicotinate) of 61 ± 15 μm width and 1.7 ± 0.4 mm length. Powder X-ray diffraction (PXRD) analysis of **1m** and **2m** confirm that both materials show the structures already reported for single crystals of $[Cu(\mu_3\text{-}I)(ANP)]_n$ and $[Cu(\mu_3\text{-}I)(EtIN)]_n$,[23] which consist of 1D-CPs with the copper(I) centre in a tetrahedral environment coordinated to the iminic nitrogen of ANP or EtIN terminal ligands and to three bridging iodides giving rise to Cu_2I_2 double chains (Figure 1a and 2a).

In case of $[Cu(\mu_3\text{-}I)(ANP)]_n$ the H-bonding acceptor character of the nitro-substituent of the 2-amino-5-nitropyridine ligand plays an important role in its supramolecular structure allowing the assembly of adjacent chains by formation of hydrogen bonds between the NH_2 donor groups and NO_2 acceptor groups of the neighbouring chains,[25] while the ethoxy group of ethyl-isonicotinate ligand in $[Cu(\mu_3\text{-}I)(EtIN)]_n$ precludes a suitable approach of the chains then avoiding the formation of hydrogen interchains bonds.[23]

To have control over size and shape, a rational study of the reaction parameters such as procedure of reactants combination (magnetic stirring *vs* ultrasound), reaction time, solvents and concentration of reactants has been carried out.

Nanostructure preparation and characterization

The preparation of nanostructures of $[Cu(\mu_3\text{-}I)(ANP)]_n$ (**1n**) and $[Cu(\mu_3\text{-}I)(EtIN)]_n$ (**2n**) is achieved in a one-pot synthesis. Thus, **1n** and **2n** are obtained from a solution of the reactants in acetonitrile-ethanol 2:1 and just acetonitrile, respectively, within a minute. PXRD and thermogravimetic analysis confirm that both **1n** and **2n** correspond to the structures reported for their single crystals (Figures S1-S4).
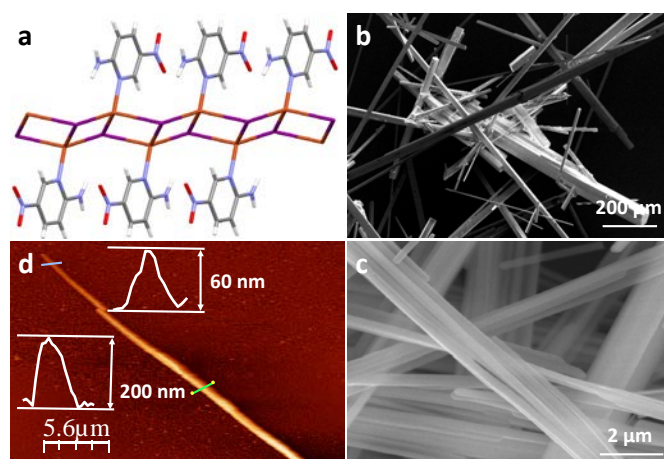
The large differences found in the size of **1n** and **2n** with their respective microcrystals have been confirmed by AFM and SEM images (Figures 1b-d and 2b-d). The low magnification of AFM and SEM images reveals that the precipitates consist of a quantity of uniform and well dispersed 1D nanostructures (Figures S5-S8). Thus, SEM images of **1n** show a nanofibrillary structure with lengths longer than 100 μm and widths in the range 0.348 ± 0.175 μm, while **2n** consists of nanoribbons with dimensions 60 ± 28 μm in length and 3 ± 2 μm in width. The morphology was confirmed by AFM which allows determining the heights of both **1n**, in the range 50-250 nm, and **2n**, in the range 6-25 nm.

Influence of ultrasound, reaction time and solvent concentration mediated synthesis over the $[Cu(\mu_3\text{-}I)(ANP)]_n$ and $[Cu(\mu_3\text{-}I)(EtIN)]_n$ nanofibres and nanoribbons morphology and size.

Table 1 collects the results obtained using different reaction conditions.

Starting with magnetically stirring variations in the reaction time do not favour aggregation in **1n**, but **2n** is slightly broadened (Figures S5 and S7, Table 1 experiments *a1*, *b1*, *a2* and *b2*). Additionally, the variation in the reactants concentration shows that an increase of concentrations produces a slight increase in the fibres width in **1n**, but no changes in **2n** (Table 1 experiments *b1, c1*, *b2* and *c2*). Although it has been described that high reactant concentration leads to high supersaturation, which results in a faster nucleation rate and thereby smaller particles; high supersaturation also speeds up agglomeration promoting production of bigger particles This enhancement in the width of **1n** can indicates that agglomeration prevails over nucleation at high reactant concentrations.[26] This aggregation is favoured in CP **1n** due to its possibility to form intermolecular H-bonds.

Table 1. Effect of the reaction time, concentration, solvent and stirring method in the widths of $[Cu(\mu_3\text{-I})(ANP)]_n$ (**1**) nanofibres and $[Cu(\mu_3\text{-I})(EtIN)]_n$ (**2**) nanoribbons at 20 °C for magnetic stirring and between 20 and 30 °C for ultrasound bath.

Exp.	reaction method	Solvent	Reaction Time (min.)	[CuI] and [ANP] or [EtIN] mM	Mean fibre width (µm)	Mean fibre length (µm)
a1	Magnetic stirring	CH₃CN/EtOH	1	35	0.3 ± 0.2	>100
b1	Magnetic stirring	CH₃CN/EtOH	9	35	0.3 ± 0.1	>100
c1	Magnetic stirring	CH₃CN/EtOH	9	70	0.5 ± 0.1	>100
d1	Ultrasound bath	CH₃CN/EtOH	1	35	0.3 ± 0.2	>100
e1	Ultrasound bath	CH₃CN/EtOH	9	35	1.3 ± 0.7	>100
f1	Ultrasound bath	CH₃CN/EtOH	9	70	2 ± 1	>100
g1	Ultrasound bath	CH₃CN/H₂O	9	35	0.6 ± 0.4	65 ± 28
a2	Magnetic stirring	CH₃CN	1	35	3 ± 2	60 ± 28
b2	Magnetic stirring	CH₃CN	9	35	7 ± 3	31 ± 18
c2	Magnetic stirring	CH₃CN	9	70	7 ± 2	20 ± 4
d2	Ultrasound bath	CH₃CN	1	35	7 ± 2	23 ± 5
e2	Ultrasound bath	CH₃CN	9	35	5 ± 3	46 ± 5
f2	Ultrasound bath	CH₃CN	9	70	9 ± 3	22 ± 7
g2	Ultrasound bath	CH₃CN/H₂O	9	35	2 ± 0.6	9±2

The means and standard deviations were calculated from values corresponding to 60 fibres (**1**) or ribbons (**2**).
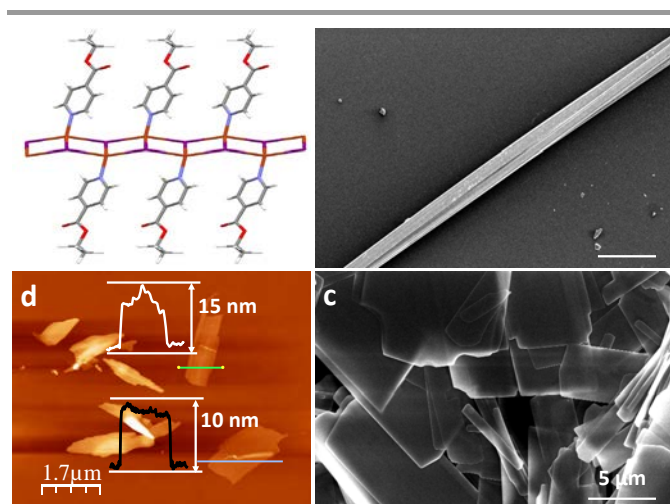
Figure 2. (a) Structure of a $[Cu(\mu_3\text{-I})(EtIN)]_n$ (**2m**) chain. Grey: C; white: H; blue: N; red: O; orange: Cu; purple: I. SEM images of microcrystals of $[Cu(\mu_3\text{-I})(EtIN)]_n$ (**2m**) (b) and **2n** nanoribbons (c). (d) AFM image of **2n** nanoribbons deposited on SiO₂ by drop-casting and their height profiles (insets).

Finally, the most significant change is observed in the width of **1n** when ultrasound is used *vs* magnetic stirring for their preparation. Table 1, experiment *b1 versus e1*, shows a more significant enhancement which is even more prominent when higher reactants concentrations are used in agreement with our previous observations, experiment *e1 versus f1* (Figure S5c). In order to rationalize this observation it has to be taken into account that ultrasound can induce supramolecular self-assembly for molecules showing donor-acceptor H-bonding sites.[27, 28] Even though the process it is still not fully understood; it is suggested in the literature that sonication and time provide suitable energy to favour intramolecular H bonds speed formation.[28, 29] Our experiments for **1n** are in agreement with this observation. Thus, longer sonication times induce fibre aggregation probably as a consequence of a slight increase in the reaction temperature, from 20 to 30 °C, upon sonication. This produces an increase in the hydrogen bonds speed formation (Table 1, experiments a1 and *e1*). Moreover, saturation also speeds up agglomeration promoting production of bigger particles (experiments *e1* and *f1)*. The effect of sonication on the widths of the nanofibres in compound **1n** is not observed for compound **2n**. This is expected since this compound does not have the capacity to

form intermolecular hydrogen bonds and helps us confirm our theory (Table 1, experiments *a2, b2, c2, d2, e2, f2*)

Although the changes in the reaction parameters (ultrasound *vs* magnetic agitation, reaction time and concentration) did not show significant effect on the length of **1n** and **2n** , the use of a mixture of solvents containing water (CH$_3$CN:H$_2$O; 1:1) for these reactions produces a significant decrease in the lengths of **1n** and **2n** (Table 1, experiments *g1 and g2*). Therefore, the use of a poor solvent seems to play a central role in the fast precipitation of the CPs once they are formed in these water containing media. Indeed, size reduction using a poor solvent is well-known for nanoparticles of CP, including MOFs; however, it is little studied for CPs with one-dimensional structures.[30, 31]

*Evolution of **1n** and **2n** nanostructures through time in their reaction medium*

The presence of functional groups with hydrogen bonds capacity and molecular recognition capability in the [Cu(μ_3-I)(ANP)]$_n$, produces a different behaviour with the reaction time compared to that observed for the [Cu(μ_3-I)(EtIN)]$_n$ in which chains do not interact through *via* H-bonds. Thus, when the suspensions of **1n** and **2n** obtained at 500 rpm for 9 min., using concentrations of the two reagents of 35 mM in acetonitrile ethanol 2:1 (compound **1n**) or just in acetonitrile, **2n**, are allowed to react for a period of a week, a widening of the fibres of the **1n** can be observed probably as a result of the formation of hydrogen bonds between them (Figures S9 and S10). However, compound **2n** nanoribbons do not suffer significant changes in their dimensions over reaction time, as expected based on the absence of H-bond capabilities in its structure. Moreover, [Cu(μ_3-I)(EtIN)]$_n$ is more insoluble than [Cu(μ_3-I)(ANP)]$_n$ in its reaction medium, so nanoribbons with a fixed size are formed immediately.

*Effect of acetic acid vapours on **1n***

The flexible structure of [Cu(μ_3-I)(ANP)]$_n$ and the presence of ANP as ligand, with available donor and acceptor H-bond groups makes this CP a potential stimuli-response material. Thus, when a microcrystalline powder of [Cu(μ_3-I)(ANP)]$_n$ is immersed in glacial acetic acid, a sorption process takes place, and the crystals change from yellow to orange, becoming amorphous. Noticeable, this is a reversible change giving rise the original microcrystals upon exposition of the amorphous material to air.[25] The change in the electrical conductivity of [Cu(μ_3-I)(ANP)]$_n$ upon exposition to vapours of different molecules was also studied confirming a selective recognition of those molecules showing H-bonding donor capabilities, including acetic acid.[32] Moreover, the structure of [Cu(μ_3-I)(ANP)]$_n$·CH$_3$COOH confirmed the hydrogen bonds interactions between the NH$_2$ functional group of the ANP and the carboxylic group of the acetic acid.[25] The ability of [Cu(μ_3-I)(ANP)]$_n$ to respond to this chemical external stimulus is attributed to the softness of the double Cu$_2$I$_2$ chains, which makes these chains very dynamic, leading to significant structural changes that translate to its electrical conductivity. Thus the ANP terminal ligand directly connected to the Cu$_2$I$_2$ chains acts as an antenna for the external chemical stimulus.
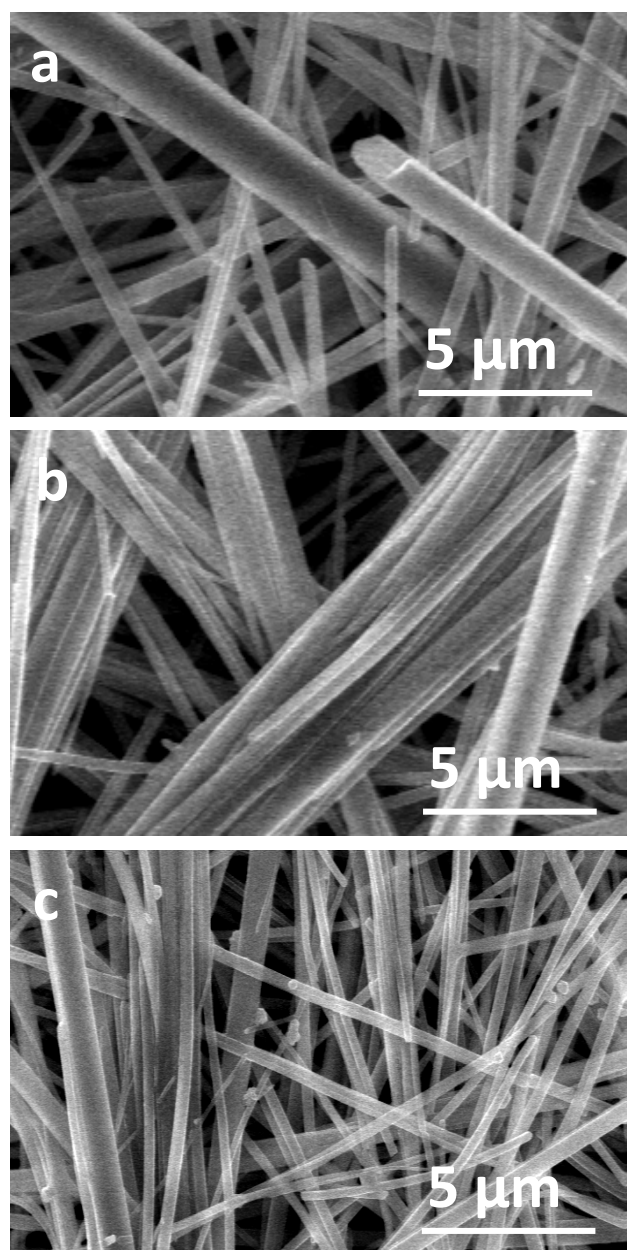
Figure 3. (a) SEM image of [Cu(μ_3-I)(ANP)]$_n$ nanofibres after being exposed to AcOH vapours for 72 h. (b) SEM image of the same nanofibres exposed to AcOH vapours upon standing in air for 30 d. (c) SEM image of the same nanofibres exposed to AcOH vapours upon standing in air for 30 d and heated at 50 ºC for 2 h.

In order to analyse possible morphological changes in **1n** induced by the presence of acetic acid vapours, a sample of **1n** was exposed to acetic acid vapours for 72 h. The new **1n**×HAcO material was characterized by elemental analysis, IR, X-ray powder diffraction and SEM. Elemental analysis quantify a HAcO adsorption of *ca*. 10 %wt. The IR spectrum of **1n**×HAcO shows one additional band to those observed in the initial material at 1715 cm^{-1}, indicative of the presence of acetic acid. Although X-ray powder diffraction does not show any significant changes (Figure 3 and Figure S11), the morphology of the fibres after exposition to acetic acid changed, with their

widths doubled to 740 ± 468 nm. Consequently, acetic acid links to the ANP terminal ligands *via* hydrogen bonding interactions, favouring the broadening of the fibres but without changing their crystal structure. It is worth mentioning that, on the one hand, the crystallinity of the nanofibers upon acetic acid exposition is intact and that the diffraction pattern agrees to that shown for **1m** (Figure S12). Therefore, our hypothesis of the interaction between **1n** and HAcO molecules is taken place at the surface of the nanofibers leading to an enhancement in the width while retaining its atomic structure. Finally, the reversibility of the acetic acid adsorption by **1n** was studied. Thus **1n×HAcO** was allowed to stay in air for 30 days. The SEM characterization of the new material shows lateral dimensions of 600 ± 497 nm which are slightly thinner in width than **1n×HAcO** but wider than the initial **1n**. IR spectrum at this state still shows the vibration assigned to the carboxylic group (Figure S13). Desorption of HAcO molecules from **1n×HAcO** is fully completed upon heating at 50 ^{0}C for 2 hours. IR spectroscopy confirms the absence of carboxylic groups (Figure S13). Morphological characterization of the desorbed crystalline material shows widths of 443 ± 332 nm (Figure 3) which compares with those observed in the initial non-treated **1n** fibres.

Conclusions

The integrity of the double-chain structures of **1** and **2** is directed by the dynamic Cu-I coordination bonds, however additional supramolecular H-bonds act packing double-chains in **1**. Therefore, the aggregation to produce large nanostructures in these CPs will be dominated by the thermodynamic equilibrium of the systems while shortening of these structures will be achieved under kinetic control in the formation reaction. Additionally, in **1** the thermodynamic vs kinetic could allow a control of the width of the material. These are important considerations towards the modification of synthetic experimental parameters to gain control over the material dimensions. Indeed, we have observed that it is possible to modulate the dimensions of both materials upon slight selected changes in some experimental parameters. Thus, modification of the energetic reaction conditions in the preparation of **1** (magnetic agitation *versus* sonication) produces a widening under more energetic conditions when either the time (Table 1, experiment *d1 vs e1*) or concentration (Table 1, experiment *e1 vs f1*) enhance, at the time that the length is over hundreds of microns, leading to morphologies thermodynamically controlled. In the case of compound **2**, thermodynamically controlled material undergoes a clear increase in the length while the width, dominated only by Van der Waals interactions, is almost unaffected. Here, at short reaction times, more energetic conditions favour the kinetic control over the thermodynamic one; at longer reaction times the thermodynamic control occurs, whereas higher reactant concentrations produce the kinetic control, due to the high insolubility of this CP (Table 1, experiment *a2 vs d2*, *b2 vs e2* and *c2 vs f2*).

It is worth mentioning that in both reactions the increase in the concentration produces a fast precipitation; this induces a kinetically controlled material, therefore leading to a reduction in the length of the structures for **2**. However, this also favours the formation of H-bonds, hence a thermodynamically controlled material and an increase in the width of the fibres for **1**. Similar results are obtained when water, a poor solvent, is incorporated in both reactions: kinetically controlled structures are obtained leading to reduction in shortening of the structures of **1** and **2**.

To sum up, by means of a simple method, in a single step at room temperature based on the high insolubility in the reaction medium of the PCs **1** and **2**, we can control the dimensions of the fibres of one-dimensional coordination polymers of Cu(I) with different types of terminal ligands.

The presence of organic ligands with molecular recognition capability able to form H-bonds, as in **1**, is a key to create sensors for compounds with H-bonds capacity. In this context, we have showed the effect of acetic acid vapours to aggregate fibres of **1n** in a reversible way. Since the selected CPs of this study show luminescent properties, they could act as sensors to detect volatile organic compounds. Additionally, their control of size could allow their integration in opto-electronic nanodevices for sensing.

We envision that studies focusing on the reduction and control of size in CPs are still necessary to gain knowledge and allow the processability of this novel materials for the construction of nanodevices.

This work provides preliminary results in the nanoprocessing of two functional PCs showing that small modifications in the reaction conditions (time, agitation method, solvent, concentration of reagents, etc.) lead to significant changes in the final material dimensions.

Experimental Section

Materials and Methods

All reagents and solvents were purchased from standard chemical suppliers and used as received.

IR spectra were recorded on a PerkinElmer 100 spectrophotometer using a PIKE Technologies MIRacle Single Reflection Horizontal ATR Accessory from 4000-600 cm^{-1}. Elemental analysis was performed on an LECO CHNS-932 Elemental Analyzer. Powder X-ray diffraction has been collected using a Diffractometer PANalyticalX'Pert PRO θ/2θ primary monochromator and detector with fast X'Celerator. The samples have been analysed with scanning θ/2θ. SEM images were measured with a Philips XL30 S-FEG scanning electron microscope.

*SEM samples preparation of [Cu(μ$_3$-I)(ANP)]$_n$ (**1n**)*. A mixture of 0.53 mmol of copper(I) iodide dissolved in 10 mL of acetonitrile and 0.53 mmol of 2-amino-5-nitropyridine (ANP) dissolved in 5 mL of ethanol was magnetically stirred (500 rpm) at 20 ^{0}C. After 1 min., an orange suspension was formed. 20 µL of this suspension were dispersed onto freshly prepared (15 min sonicated in acetone and 15 min sonicated in 2-

propanol) doped SiO_2 substrates and left to adsorb until the drop completely evaporated (15 min.). The samples were covered with a 10 nm-thick layer of conductive Cr to improve the resolution of the images.

SEM samples preparation of [Cu(μ₃-I)(EtIN)]ₙ (2n). A mixture of 0.53 mmol of copper(I) iodide dissolved in 15 mL of acetonitrile and 0.53 mmol of ethyl isonicotinate (EtIN) was magnetically stirred (500 rpm) at 20 ^{0}C. After 1 min., a yellow suspension was formed. 20 μL of this suspension were dispersed onto freshly prepared (15 min sonicated in acetone and 15 min. sonicated in 2-propanol) glass substrates and left to adsorb until the drop completely evaporated (15 minutes). The samples were covered with a 10 nm-thick layer of conductive Cr to improve the resolution of the images.

AFM samples preparation of [Cu(μ₃-I)(ANP)]ₙ (1n). A mixture of 0.53 mmol of copper(I) iodide dissolved in 10 mL of acetonitrile and 0.53 mmol of 2-amino-5-nitropyridine (ANP) dissolved in 5 mL of ethanol was magnetically stirred (500 rpm) at 20 ^{0}C. After 1 min., an orange suspension was formed. 40 μL of this suspension were diluted with 3960 μL of bidistilled water, and 15 μL of the new suspension were drop-cast onto freshly prepared (15 min sonicated in acetone and 15 min. sonicated in 2-propanol) doped SiO_2 substrates. After 3 min. of adsorption, the surfaces were dried under an Argon flow.

AFM samples preparation of [Cu(μ₃-I)(EtIN)]ₙ (2n). A mixture of 0.53 mmol of copper(I) iodide dissolved in 15 mL of acetonitrile and 0.53 mmol of ethyl isonicotinate (EtIN) was magnetically stirred (500 rpm) at 20 ^{0}C. After 1 min., a yellow suspension was formed. 400 μL of this suspension were diluted with 3600 μL of bidistilled water, and 15 μL of the new suspension were drop-cast onto freshly prepared (15 min sonicated in acetone and 15 min sonicated in 2-propanol) doped SiO_2 substrates. After 3 minutes of adsorption, the surfaces were dried under an argon flow.

Atomic Force Microscopy (AFM) images were acquired in dynamic mode using a Nanotec Electronica system operating at room temperature in ambient air conditions. For AFM measurements, Olympus cantilevers were used with a nominal force constant of 0.75 N/m and a resonance frequency of about 70 kHz. The images were processed using WSxM.[33] The surfaces used for AFM were SiO_2 300 nm thickness (IMS Company). SiO_2 surfaces were sonicated in ultrasound bath at 37 kHz and 380 W, for 15 min. in acetone, 15 min. in 2-propanol and then dried under an argon flow.

Synthetic procedures

Synthesis of [Cu(μ₃-I)(ANP)]ₙ (1m). Orange needle-like microcrystals of this coordination polymer have been prepared following the method already described in the literature.[25]

Synthesis of nanostructures of [Cu(μ₃-I)(ANP)]ₙ (1n). Two solutions of 0.53 mmol (100 mg) of copper(I) iodide in 10 mL of acetonitrile and 0.53 mmol (73 mg) of 2-amino-5-nitropyridine (ANP) in 5 mL of ethanol were prepared at 30 ^{0}C, and then mixed with magnetic stirring at 500 rpm. Immediately, the solution turned from yellow to orange and a solid precipitate as nanocrystals after 1 min. The solid was filtered off and dried

in vacuum. Yield: 62 mg, 26 % based on Cu. Elemental analysis Calcd (found) % for $C_5H_5CuIN_3O_2$: C 18.22 (18.90), H 1.53 (1.60), N 12.75 (12.93); Selected IR data $\overline{\nu}$ (cm^{-1}): 3444 (m), 3323 (m), 3087 (w), 3056 (w), 1625 (s), 1601 (m), 1570 (m), 1491 (s), 1421 (m), 1329 (s), 1285 (s), 1161 (w), 1124 (m), 941 (m), 869 (w), 826 (vs), 760 (m), 723 (m), 667 (w). The homogeneity of the sample was confirmed by X-ray powder diffraction (Figure S1).

Synthesis of nanostructures of [Cu(μ₃-I)(ANP)]ₙ (1n) in aqueous medium. Two solutions of 0.53 mmol (100 mg) of copper(I) iodide in 15 mL of acetonitrile and 0.53 mmol (73 mg) of 2-amino-5-nitropyridine (ANP) in 15 mL of distilled water were prepared at 30 ^{0}C, and then mixed in an ultrasound bath (Elma, 37 kHz, 380 W). Immediately, the solution turned from yellow to orange and a solid precipitate as nanocrystals after 1 min. After 9 minutes, the solid was filtered off and dried in vacuum. Yield: 137 mg, 58 % based on Cu. Elemental analysis Calcd (found) % for $C_5H_5CuIN_3O_2$: C 18.22 (18.90), H 1.53 (1.60), N 12.75 (12.93); Selected IR data $\overline{\nu}$ (cm^{-1}): 3444 (m), 3323 (m), 3087 (w), 3056 (w), 1625 (s), 1601 (m), 1570 (m), 1491 (s), 1421 (m), 1329 (s), 1285 (s), 1161 (w), 1124 (m), 941 (m), 869 (w), 826 (vs), 760 (m), 723 (m), 667 (w). The homogeneity of the sample was confirmed by X-ray powder diffraction (Figure S1).

Synthesis of [Cu(μ₃-I)(EtIN)]ₙ (2m). Yellow needle-like microcrystals were obtained following the method described in the literature.[23]

Synthesis of nanostructures of [Cu(μ₃-I)(EtIN)]ₙ (2n). Yellow submicron and nanocrystals of this compound have been prepared by variation the method previously reported.[23] To a 15 mL of an acetonitrile solution of copper(I) iodide, 0.53 mmol (100 mg), 0.53 mmol (80 μL) of ethyl-isonicotinate (EtIN) were added and magnetically stirred at 500 rpm. Immediately, a yellow solid was formed. The solid was filtered off and dried in vacuum. Yield: 110 mg, 61 % based on Cu. Elemental analysis Calcd (found) % for $C_8H_9CuINO_2$: C 28.13 (28.20), H 2.66 (2.44), N 4.10 (4.02); Selected IR data $\overline{\nu}$ (cm^{-1}): 3421 (w), 1716 (m), 1556 (w), 1414 (s), 1394 (w), 1363 (m), 1322 (m), 1288 (s), 1257 (m), 1226 (w), 1135 (w), 1114 (w), 1061 (m), 1018 (m), 856 (w), 759 (m), 698 (m). The homogeneity of the sample was confirmed by X-ray powder diffraction (Figure S2).

Synthesis of nanostructures of [Cu(μ₃-I)(EtIN)]ₙ (2n) in aqueous medium. To a 15 mL of an acetonitrile solution of copper(I) iodide, 0.53 mmol (100 mg), 0.53 mmol (80 μL) of ethyl-isonicotinate (EtIN) in 15 mL of distilled water were added and mixed in an ultrasound bath (Elma, 37 kHz, 380 W). Immediately, a yellow solid was formed. After 9 minutes, the solid was filtered off and dried in vacuum. Yield: 112 mg, 62 % based on Cu. Elemental analysis Calcd (found) % for $C_8H_9CuINO_2$: C 28.13 (28.20), H 2.66 (2.44), N 4.10 (4.02); Selected IR data $\overline{\nu}$ (cm^{-1}): 3421 (w), 1716 (m), 1556 (w), 1414 (s), 1394 (w), 1363 (m), 1322 (m), 1288 (s), 1257 (m), 1226 (w), 1135 (w), 1114 (w), 1061 (m), 1018 (m), 856 (w), 759 (m), 698 (m). The homogeneity of the sample was confirmed by X-ray powder diffraction (Figure S2).

Conflicts of interest

There are no conflicts to declare".

Acknowledgements

Notes and references

1. S. R. N. Batten, S. M.; Turner, D. , *RSC Publishing,*, 2009, **7**.
2. P. Amo-Ochoa, S. S. Alexandre, S. Hribesh, M. A. Galindo, O. Castillo, C. J. Gómez-García, A. R. Pike, J. M. Soler, A. Houlton and F. Zamora, *Inorg. Chem.*, 2013, **52**, 5290-5299.
3. P. Amo-Ochoa, O. Castillo, S. S. Alexandre, L. Welte, P. J. de Pablo, M. Isabel Rodriguez-Tapiador, J. Gomez-Herrero and F. Zamora, *Inorg. Chem.*, 2009, **48**, 7931-7936.
4. X.-C. Shan, F.-L. Jiang, L. Chen, M.-Y. Wu, J. Pan, X.-Y. Wan and M.-C. Hong, *J. Mater. Chem. C*, 2013, **1**, 4339-4349.
5. C. Y. K. Chan, J. W. Y. Lam, Z. Zhao, S. Chen, P. Lu, H. H. Y. Sung, H. S. Kwok, Y. Ma, I. D. Williams and B. Z. Tang, *J. Mater.Chem. C*, 2014, **2**, 4320-4327.
6. Q. Qi, J. Zhang, B. Xu, B. Li, S. X.-A. Zhang and W. Tian, *The J. Phys.Chem. C*, 2013, **117**, 24997-25003.
7. V. G. Vegas, R. Lorca, A. Latorre, K. Hassanein, C. J. Gómez-García, O. Castillo, Á. Somoza, F. Zamora and P. Amo-Ochoa, *Angew. Chem. Inter. Ed.*, 2017, **56**, 987-991.
8. P. Amo-Ochoa and F. Zamora, *Coord. Chem.Rev.*, 2014, **276**, 34-58.
9. W. X. Zhang, T. Shiga, H. Miyasaka and M. Yamashita, *J. Am. Chem. Soc.*, 2012, **134**, 6908-6911.
10. X. H. Wang, H. J. Chang, J. Xie, B. Z. Zhao, B. T. Liu, S. L. Xu, W. B. Pei, N. Ren, L. Huang and W. Huang, *Coord. Chem. Rev.*, 2014, **273**, 201-212.
11. G. Beobide, O. Castillo, J. Cepeda, A. Luque, S. Perez-Yanez, P. Roman and J. Thomas-Gipson, *Coord. Chem. Rev.*, 2013, **257**, 2716-2736.
12. G. Givaja, P. Amo-Ochoa, C. J. Gomez-Garcia and F. Zamora, *Chem. Soc. Rev.*, 2012, **41**, 115-147.
13. P. Amo-Ochoa, O. Castillo, C. J. Gomez-Garcia, K. Hassanein, S. Verma, J. Kumar and F. Zamora, *Inorg. Chem.*, 2013, **52**, 11428-11437.
14. B. Xiao, P. J. Byrne, P. S. Wheatley, D. S. Wragg, A. Zhao, A. J. Fletcher, K. M. Thomas, L. Peters, S. O. EvansJohn, J. E. Warren, W. Zhou and R. E. Morris, *Nat. Chem.*, 2009, **1**, 289-294.
15. F. Zamora, M. P. Amo-Ochoa, P. J. S. Miguel and O. Castillo, *Inorg. Chim. Acta*, 2009, **362**, 691-706.
16. D. Rodriguez-San-Miguel, P. Amo-Ochoa and F. Zamora, *Chem. Commun.*, 2016, **52**, 4113-4127.
17. C. Neaime, C. Daiguebonne, G. Calvez, S. Freslon, K. Bernot, F. Grasset, S. Cordier and O. Guillou, *Chem. – A Eur. J.*, 2015, **21**, 17466-17473.
18. C. Hermosa, B. R. Horrocks, J. I. Martinez, F. Liscio, J. Gomez-Herrero and F. Zamora, *Chem. Sci.*, 2015, **6**, 2553-2558.
19. G. Das, B. P. Biswal, S. Kandambeth, V. Venkatesh, G. Kaur, M. Addicoat, T. Heine, S. Verma and R. Banerjee, *Chem. Sci.*, 2015, **6**, 3931-3939.
20. K. Liu, Z.-R. Shen, Y. Li, S.-D. Han, T.-L. Hu, D.-S. Zhang, X.-H. Bu and W.-J. Ruan, *Sci. Reports*, 2014, **4**, 6023.
21. P. G. Derakhshandeh and J. Soleimannejad, *Ultrason. Sonochem..*, 2016, **31**, 122-128.
22. V. Vegas, M. Villar-Alonso, C. Gómez-García, F. Zamora and P. Amo-Ochoa, *Polymers*, 2017, **9**, 565.
23. K. Hassanein, J. Conesa-Egea, S. Delgado, O. Castillo, S. Benmansour, J. I. Martinez, G. Abellan, C. J. Gomez-Garcia, F. Zamora and P. Arno-Ochoea, *Chem.-Eur. J*, 2015, **21**, 17282-17292.
24. Q. Benito, X. F. Le Goff, S. Maron, A. Fargues, A. Garcia, C. Martineau, F. Taulelle, S. Kahlal, T. Gacoin, J.-P. Boilot and S. Perruchas, *J. Am. Chem. Soc.*, 2014, **136**, 11311-11320.
25. P. Amo-Ochoa, K. Hassanein, C. J. Gomez-Garcia, S. Benmansour, J. Perles, O. Castillo, J. I. Martinez, P. Ocon and F. Zamora, *Chem. Commun.*, 2015, **51**, 14306-14309.
26. Y. Dong, W. K. Ng, J. Hu, S. Shen and R. B. H. Tan, *Int. J. Pharm.*, 2010, **386**, 256-261.
27. J. Shen, P. Ding, L. Gao, Y. Gao, Q. Zhang, S. Yuan and X. Xin, *Coll. Poly. Sci.*, 2017, **295**, 1765-1772.
28. I. Maity, D. B. Rasale and A. K. Das, *Soft. Matter.*, 2012, **8**, 5301-5308.
29. M. Rastogi, A. Awasthi and J. P. Shukla, *Phys. Chem. Liq.*, 2004, **42**, 117-126.
30. L. r. Meng, R. Mo, H. Zhou, G. Wang, W. Chen, D. Wang and Q. Peng, *Cryst. Growth. Des.*, 2010, **10**, 3387-3390.
31. R. Kumar and P. F. Siril, *J.Nanoparticle Research*, 2015, **17**, 256.
32. K. Hassanein, P. Amo-Ochoa, C. J. Gomez-Garcia, S. Delgado, O. Castillo, P. Ocon, J. I. Martinez, J. Perles and F. Zamora, *Inorg. Chem.*, 2015, **54**, 10738-10747.
33. M. Usman, S. Mendiratta and K. L. Lu, *Adv. Mater.*, 2017, **29**.